Evidence of dislocation loop preferential nucleation in irradiated aluminum under stress

D. da Fonseca, F. Mompiou, T. Jourdan, J.-P. Crocombette, A. Chartier, F. Onimus

D. Da Fonseca, F. Mompiou, T. Jourdan, J.-P. Crocombette, A. Chartier, F. Onimus, Evidence of dislocation loop preferential nucleation in irradiated aluminum under stress, Scripta Materialia, Volume 233, 2023,115510,

https://doi.org/10.1016/j.scriptamat.2023.115510

Evidence of dislocation loop preferential nucleation in irradiated aluminum under stress

D. Da Fonseca[1,5], F. Mompiou[4,5], T. Jourdan[1], J.-P. Crocombette[1], A. Chartier[3], and F. Onimus[2,*]

[1]Université Paris-Saclay, CEA, Service de recherche en Corrosion et Comportement des Matériaux, SRMP, F-91191 Gif-sur-Yvette, France
[2]Université Paris-Saclay, CEA, Service de Recherche en Matériaux et procédés Avancés, F-91191 Gif-sur-Yvette, France
[3]Université Paris-Saclay, CEA, Service de recherche en Corrosion et Comportement des Matériaux, F-91191 Gif-sur-Yvette, France
[4]Centre d'Elaboration de Matériaux et d'Etudes Structurales, CNRS UPR 8011, 29 rue J. Marvig, BP 94347, Toulouse cedex 4 31055, France
[5]Université de Toulouse, UPS, F-31055 Toulouse, France
[*]Corresponding author : fabien.onimus@cea.fr

Abstract

To explain irradiation creep, several mechanisms have been proposed. Some are based on the effect of stress on either nucleation or growth of dislocation loops. To investigate these mechanisms in aluminum we combine in-situ transmission electron microscope irradiation under stress and two simulation approaches (object kinetic Monte-Carlo, molecular dynamics Frenkel pair accumulation). We observe the selectivity of Frank loop variants under electron irradiation and applied stress. When the stress is turned on after loop formation, there is no loop variant selectivity, suggesting the absence of preferential absorption on already formed loops. Object kinetic Monte-Carlo simulations, including the effect of stress on the diffusion of point defects, show no growth rate difference between loop variants. Frenkel pair accumulation simulations exhibit variant selectivity of nucleated loops. This shows that loop selectivity is due to preferential nucleation of well oriented loops under stress and not to differential growth of loops.

Keywords— irradiation creep, dislocation loop, in-situ straining irradiation, object kinetic Monte-Carlo, Frenkel pair accumulation

Under irradiation and applied stress, a specific deformation process known as irradiation creep arises in many materials, such as steels, nickel-based and zirconium alloys [20, 23, 33]. Its phenomenology, well documented, is very different from thermal creep, which essentially operates at high temperature. Depending on irradiation flux, temperature and stress magnitude, irradiation creep can be responsible for deformation rates far higher than those related to thermal creep [30]. Understanding the mechanisms underlying irradiation creep is therefore of prime importance.

Several mechanisms have been proposed to explain irradiation creep [28, 2, 33]. Some of them are based on the effect of stress on dislocation loops and account for various observations. In some experiments, interstitial loops

in planes where the normal stress is the largest have been shown to be larger [3, 21], resulting in a net strain. Other experiments have evidenced an increase in interstitial loop density with the normal stress on the loop habit planes, also resulting in a net strain [32, 3, 5, 40, 42, 47]. The mechanisms which can explain such results can be classified in two main categories: the stress-induced preferred absorption (SIPA) phenomenon [19, 4] and the stress-induced preferred nucleation (SIPN) of interstitial dislocation loops. SIPA is due to the anisotropic diffusion of self-interstitials and vacancies under stress [45, 11]. It has been shown to be able to explain not only differential loop growth, but also preferential loop formation in some planes [44]. The first version of SIPN was based on the classical nucleation theory, which proved erroneous for interstitial dislocation loops due to the absence of activation barrier for nucleation [15]. Later, it was suggested that the reorientation of small SIA clusters under stress could explain the different loop densities on different habit planes [43]. However, the magnitude of this effect was found too low to match experimental results. Although this process is not a classical nucleation process, we consider it as SIPN, as opposed to the purely diffusive SIPA process.

Whether the contribution of loops to irradiation creep is due to a SIPN or a SIPA mechanism is still an open question [14]. Results are not all consistent, with some experiments leading to opposite trends to what would be expected due to SIPN [41] or SIPA [36]. In addition, internal stresses are difficult to determine and probably affect the results [17, 37, 1]. Finally, in high dose irradiations, loops interact with the dislocation network. This interaction alters the loop size distributions and makes the sole effect of stress on loops less easy to observe, especially if irradiations are performed ex-situ [16, 34, 18]. Therefore, in-situ, low dose irradiations should be preferred to investigate stress effects on loops.

In the following we combine both experimental in-situ straining transmission electron microscopy (TEM) irradiations of aluminum thin foils and two simulation methods, namely object kinetic Monte-Carlo (OKMC) and molecular dynamics using Frenkel pair accumulation (FPA) process, to determine whether stress has an impact on the nucleation and/or on the growth of loops.

In-situ observations were conducted in a JEOL 2010HC microscope operated either at 140 kV, *i.e.* well below displacement threshold for setting up experiments and at 180 kV for irradiation. A pure aluminum (99.999%) annealed 0.5 mm thick foil was used for the experiments. It ensures a large grain microstructure with a strong cube texture, *i.e.* foil normal close to [0 0 1] and rolling direction along the [1 0 0] direction. 3 mm disc specimens were extracted from the foil plane, mechanically grinded and eventually doubled-jet electropolished to electron transparency around a central hole using a solution of perchloric acid/ethanol (5/95) at -30°C and 30 V. Then the specimens were glued, with a cyanoacrylate glue, on a copper tensile grid and placed in a Gatan straining holder, as shown in Fig.1.a. Samples were oriented on the copper grid so that the $\langle 1\,1\,0\rangle$ direction (at 45° from the rolling direction) was aligned with the straining direction, with the normal of the foil close to $\langle 0\,0\,1\rangle$ direction. The stress was imposed by a micrometer controlled motion of one of the sample grip while the other one stayed at rest. The method used to evaluate the applied stress is described in Supplementary Material. Irradiations were conducted at room temperature without and with external stress. At this temperature (below 0.5 T_m, where T_m is the melting temperature), emission of point defects from loops can be neglected and the contribution of the stress dependent emission rates to loop evolution is negligible. The beam was adjusted to obtain an electron flux of 1×10^5 $\mathrm{e}^-/\mathrm{nm}^2/\mathrm{s}$ at 180 kV which corresponds to 4.55×10^{-5}dpa/s. The damage rate was computed as the electron flux times the adequate cross-section given in Oen's table [31]. In this condition, the irradiated zone covers a disk of 3 μm of diameter. Observations were made in the center of the irradiated area which was measured [29] to be around 170 nm thick (see Supplementary Material). Three experiments referenced as 1, 2 and 3 (Fig. 1.b) are detailed in the following. They were all carried out in the same grain in the area where the local stress is uniaxial and parallel to the tensile axis. Fig. 2 shows weak-beam dark field (WBDF) images taken after irradiation with $\boldsymbol{g} = 200$, using $g(3g)$ diffraction condition, in order to have all possible Frank loops visible.

After irradiation without applied stress, the microstructure was characterized in detail. The loop nature was determined using the inside/outside method [26, 13]. Only interstitial loops were observed. Furthermore, most of these loops are Frank loops with Burgers vectors $\boldsymbol{b} = 1/3\langle 1\,1\,1\rangle$ and lying in $\{1\,1\,1\}$ habit planes [48]. In the tensile configuration used, Burgers vectors $1/3[\bar{1}\,1\,1]$ and $1/3[1\,\bar{1}\,1]$ (denoted herein as type A loops in red in Fig. 1c-d) are both perpendicular to the straining axis, while Burgers vectors $1/3[1\,1\,1]$ and $1/3[1\,1\,\bar{1}]$ (denoted herein as type B loops in green in Fig. 1c-d) are tilted 35° away from the straining axis. Hence, the two types of loops are not equivalent with respect to the applied stress. For the type A loops, the component of the stress along the loop Burgers vector is equal to zero. Moreover, all the normals of the habit planes of the loops make a 55° angle with the foil normal which allows the observations of the loops with the same apparent projections, but with different orientation with respect to the tensile axis: the long axis of the ellipse of the A loops is vertical, parallel to the tensile axis while the long axis of the ellipse of the B loops is horizontal, perpendicular to the tensile axis.

Experiment 1 (Fig.2.a) is a 38 minutes stress free irradiation. It yields a proportion of 60% of type A loops

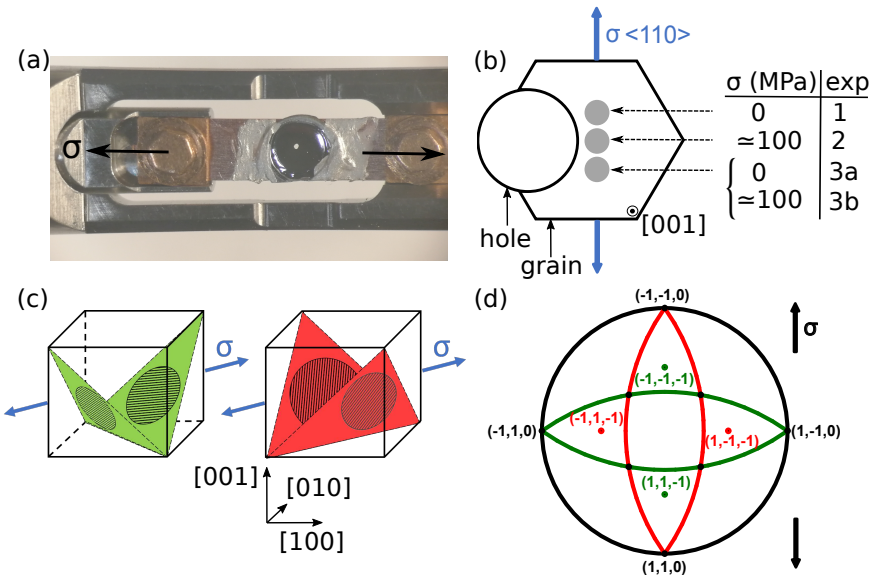

Figure 1: (a) Straining TEM sample holder, (b) sketch of the experiments: three irradiation are conducted in the same grain close to the electropolished hole, with different stress conditions (without or with stress estimated to be around 100 MPa), the final microstructures are presented in Fig. 2, (c) orientation of the two different Frank loop types with respect to the tensile axis, and (d) the corresponding stereographic projection with the associated tensile axis. Well-oriented loops are presented in green (type B) and unfavorably oriented loops are presented in red (type A). The method used to evaluate the applied stress is described in the Supplementary Material.

and 40% of type B loops. Although the proportions are not exactly equally balanced, it can be considered as a reference state. The authors want to point out that a stress-free state, with nearly balanced proportion of loops, is not systematically obtained. This is presumably due to residual stresses. Only samples with nearly stress-free state, with initially quasi-balanced proportion of loops, have thus been considered for this work.

In experiment 2, the specimen was first strained at lower voltage to avoid atomic displacement until the first dislocation motion was observed. Then, the displacement of the tensile grip was slightly reduced. Irradiation started with immobile dislocations under a stress slightly below the yield stress that can be roughly estimated from dislocation curvature, *i.e.* of the order of 100 MPa in a thin foil (see Supplementary Material). After irradiation, the tensile grip was again slightly moved (a few microns), inducing dislocation glide, in order to check that the stress did not relax during irradiation. Fig. 2.b shows the microstructure after 41 minutes of irradiation. Contrary to experiment 1, 10% of loops are of type A and 90% of type B. This result is consistent with most of the observations in literature where the populations with the largest projection of the tensile stress vector on the normal to their habit plane are preferentially formed [32, 3, 5, 17, 37, 1, 40, 47]. This strong anisotropy of loop population is a clear evidence of the influence of the applied stress, but this experiment is not self-sufficient to ascertain between preferential absorption and preferential nucleation mechanisms, as some studies explained the anisotropic population with SIPA mechanism [17, 47] based on the work of Wolfer [43].

A third experiment was hence conducted, in two steps, to discriminate between SIPA and SIPN. In a first step (experiment 3a), a new area was irradiated without applying an external stress, until the loops were large enough to allow their type classification. The irradiation was stopped after 16 minutes (see Fig.2.c). As expected for an irradiation without stress, proportions are balanced with 47% of type A loops and 53% of type B loops and a measured mean diameter of 13.3 nm and 12.4 nm, respectively. This corresponds to a mean growth rate in diameter of 0.013 nm/s. Using the same protocol as in experiment 2, the sample was then stressed and irradiated for 48 minutes in the same area (experiment 3b) (see Fig.2.d). The proportion of the loops did not significantly evolve: 40% of loops are of type A and 60% of type B. The loops have a mean diameter of 27 nm for both types.

Comparing the results of experiment 2 and 3 shows that stress has a strong impact only in early stages of irradiation, suggesting that the contribution of SIPA should be very moderate. The shrinkage of type A loops and the growth of type B loops would be expected due to SIPA but instead both types of loop grow and only the shrinkage of new small loops is observed, becoming sacrificial loops for the growth of previously formed loops. Suzuki and Sato [40] did an equivalent experiment to our experiment 3 in Fe-18Cr-14Ni alloy under 1 MeV electron

irradiation at temperature ranging between 340°C and 456°C, and they drew the same conclusion. To confirm this analysis, SIPA and SIPN were evaluated separately using two different simulation methods. The results are presented in the following.

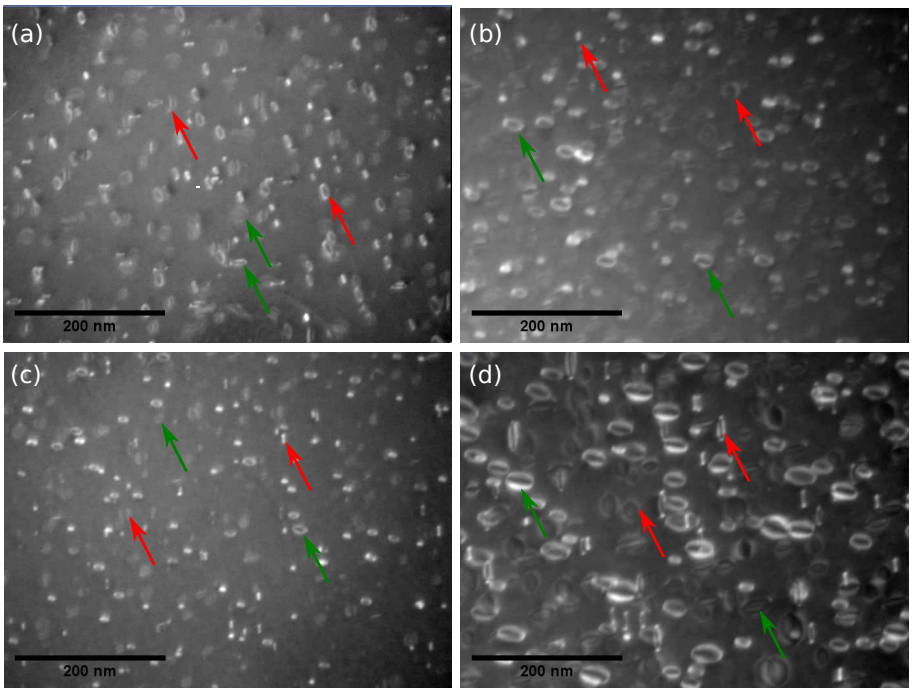

Figure 2: Irradiations conducted in the same grain with a flux of 1×10^5 $e^-/nm^2/s$ at room temperature: (a) experiment 1 without applied stress for 38 minutes, (b) experiment 2 under stress for 41 minutes, (c) experiment 3a without stress for 16 minutes, (d) experiment 3b with 48 additional minutes under stress. Red arrows point out some unfavorably oriented loops and green arrows some well-oriented loops.

In order to evaluate the role of SIPA on loop growth under experimental conditions, OKMC [12, 27, 22] simulations were used. Accordingly, the $\boldsymbol{x}$, $\boldsymbol{y}$ and $\boldsymbol{z}$ directions of the simulation box are chosen along $[1\,\bar{1}\,0]$, $[1\,1\,0]$ and $[0\,0\,1]$ directions, respectively. The dimensions of the box along these directions are 100, 100 and 200 nm. The height of 200 nm in the $\boldsymbol{z}$ direction corresponds approximately to the foil thickness. Free surfaces are hence introduced in the $\boldsymbol{z}$ direction while periodic boundary conditions are considered in $\boldsymbol{x}$ and $\boldsymbol{y}$ directions. Initially, the simulation box contains no point defect. Frenkel pairs are then generated at a dose rate of 5×10^{-5} dpa/s to mimic TEM irradiation. Point defects migrate in the simulation box and can recombine with defects of opposite type, agglomerate with each other (thus forming interstitial loops or cavities) or escape to the surfaces. In addition, immobile traps are randomly placed in the system before the irradiation starts, to mimic impurities present in the material. These impurities are assumed to strongly bind to migrating point defects. Without such traps, SIAs would all recombine with vacancies or escape to free surfaces, leaving the simulation box free of loops. A total of 10 impurities, corresponding to a concentration of 0.08 appm, is chosen to reproduce the observed loop density in experiment 3a, well below the estimated experimental concentration. This suggests that not all impurities are efficient traps for point defects. When SIAs agglomerate with an impurity to form a loop, the habit plane is chosen randomly and kept the same as the loop grows, so SIPN is purposefully discarded. More details about the parametrization are given in Supplementary Material.

The migration of point defects is affected by the internal stress generated by dislocation loops in the thin foil and the externally applied stress [22]. The elastic interaction energy between point defects and the local stress field, which biases the migration of point defects and leads to SIPA, is given by an elastic model based on the elastic dipole tensors and diaelastic polarizabilities of point defects [9]. These properties have been obtained recently in aluminum from density functional theory calculations [11]. Image forces induced by the presence of loops near surfaces [46] are neglected, as it has been shown that they affect dislocation loop growth only when loops are a few nanometers away from the surface [22].

Simulations were run at 300 K without or with a 100 MPa uniaxial stress applied in the $\boldsymbol{y}$ direction. Simulations were stopped after 10 minutes of irradiation. Cluster distributions are obtained from 100 independent simulations

carried out with different spatial distributions of impurities.

Simulations performed without stress show an almost equal proportion of type A (49.4%) and type B (50.6%) loops with mean diameters 7.67 nm and 7.99 nm respectively, leading to an average growth rate of 0.013 nm/s. This growth rate is the same as in experiment 3a, which validates our simulation method. Typical microstructures and loop size distributions when a stress is applied are shown in Fig.3.b and Fig.3.e, respectively. Proportions of type A (48.5%) and type B (51.5%) loops are still balanced with mean diameters of 8.45 nm and 9.89 nm respectively. Well-oriented loops are slightly larger, indicating only a moderate effect of the stress on differential growth. This effect is however below the experimental error and hence could not be ascertained by TEM. More importantly, the simulations fail to reproduce the strong selectivity on loop variants (Fig.3.d and Fig.3.e). These results thus suggest that the microstructure evolution under stress cannot be explained by a SIPA mechanism. They are in line with the rather small effect of stress on absorption efficiencies of dislocations derived in a previous work [11]. Absorption efficiencies of loops are found to be much more dependent on other factors, such as loop size and local loop environment.

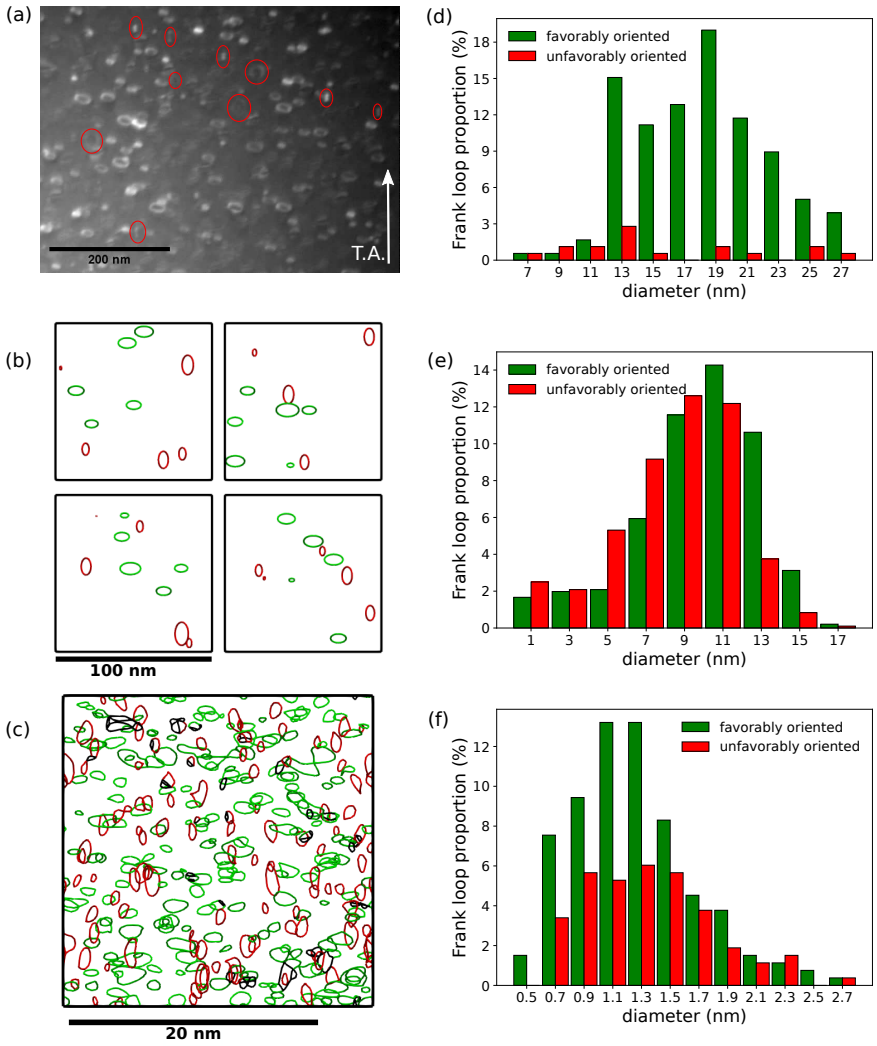

Figure 3: Comparison of the three methods to evaluate the main mechanism involved. On the left (a), (b), (c) are the microstructures studied with the same orientation of the applied stress showed by a white arrow. (a) Experiment 2: in-situ irradiation under stress, unfavorably oriented loops are in minority so some of them are highlighted by red ellipses, (b) four out of 100 systems simulated by OKMC method, (c) system simulated with FPA method, black lines correspond to non-Frank dislocations. For the simulations in (b) and (c), type A dislocations are in red and type B are in green. On the right (d), (e), (f) are the corresponding normalized distributions of loop diameters in nanometer.

To further highlight the importance of SIPN, molecular dynamics simulations of defect accumulation under stress

were performed. Simulation boxes oriented along [1 1 0], [$\bar{1}$ 1 0] and [0 0 1] directions were used. Their dimensions are of around 25x25x24 nm^3 and they contain 887520 atoms of aluminum whose interactions are described with an EAM potential [25]. Periodic boundary conditions are applied in all three directions. Simulations are done at constant room temperature and constant stress using a Berendsen thermostat and a Parrinello-Rahman barostat, with fixed angles so that the box remains tetragonal during the simulations. TEM experiments, i.e. electron irradiations, are modelled by periodically introducing Frenkel pairs in the box, following the same FPA method as in previous works [24, 35, 10, 7, 6, 8]. 200 Frenkel pairs are generated every 2 ps, which corresponds to a dose rate of 1.13×10^8 dpa/s, far from the experimental reality. The total simulated time is 0.5 ns, which makes long range diffusion negligible and therefore excludes any SIPA process. In addition, results cannot be directly compared with experiments at the same absolute value of dose. A snapshot of atomic configurations is taken every 2 ps, just before each insertion of point defects. The cell is then visualized with the OVITO software [38] and dislocations are identified with the DXA algorithm [39]. Note that only closed dislocations made up of segments with the same Burgers vector are counted in the total number of Frank loops. The evolution of loops is tracked until they are too big and interact with each other thus forming a dislocation network (around ~ 0.03 dpa).

A reference simulation was performed at zero stress. Type A loops come out at 48.6% to 51.4% for type B, thus the code reproduces correctly equiprobable loop nucleation between the two variants. In a second simulation, we set a stress of 100 MPa in [1 1 0] direction and 0 MPa in [0 0 1] and [1 $\bar{1}$ 0] directions. Under stress, we obtain the microstructure shown in Fig. 3.c and the corresponding distribution in Fig. 3.f. Among all the dislocation segments detected by OVITO, 75.8% are of Frank type (265 Frank loops are counted in Fig. 3.c). What stands out from the snapshot and the bar plot is that well-oriented loops (B type loops) are in majority (65.7% of the total). This proportion is lower than what is shown in Fig. 3.d but the result still evidences preferential orientation of Frank loops under stress (even at this relatively low applied stress for MD simulations). We found that the proportion of type B loop rises with the level of stress applied along [1 1 0] direction.

Our experiments show that the impact of stress is noticeable when it is applied from the start of the irradiation, suggesting that the anisotropic microstructure observed is due to preferential formation of well oriented loops under stress and not to the differential evolution of already existing loops. OKMC simulations confirm the small effect of SIPA and MD-FPA simulations yield an anisotropic population under stress. We thus prove that SIPN is stronger than SIPA under electron irradiation, suggesting that SIPA has only a minor contribution to irradiation creep deformation.

Acknowledgments

The authors are grateful to Estelle Meslin, Benoit Arnal and Guilhem Sagnes for their help with sample preparation and TEM operation.

References

[1] T. Atkins and R. J. McElroy. The effects of applied stress on the irradiation induced microstructures of dilute nickel alloys. In American Society for Testing and Materials, editors, Radiation-Induced Changes in Microstructure: 13th International Symposium (Part I), ASTM STP 955, page 447, 1987.

[2] V. A. Borodin. Chapter 7. irradiation induced creep. In State-of-the-art Report on Structural Materials Modelling, number NEA/NSC/R(2016)5, 2016.

[3] H. R. Brager, F. A. Garner, and G. L. Guthrie. The effect of stress on the microstructure of neutron irradiated type 316 stainless steels. J. Nucl. Mater., 66:301–321, 1977.

[4] R. Bullough and J. R. Willis. The stress-induced point defect-dislocation interaction and its relevance to irradiation creep. Philos. Mag., 31:855, 1975.

[5] D. Caillard, J. L. Martin, and B. Jouffrey. Creep under irradiation of 316 steel in the high voltage electron microscope. Acta Metall., 28:1059, 1980.

[6] A. Chartier and M.-C. Marinica. Rearrangement of interstitial defects in alpha-Fe under extreme condition. Acta Mater., 180:141–148, 2019.

[7] Alain Chartier, Gilles Catillon, and Jean-Paul Crocombette. Key role of the cation interstitial structure in the radiation resistance of pyrochlores. Phys. Rev. Lett., 102:155503, Apr 2009.

[8] Elton Y. Chen, Chaitanya Deo, and Rémi Dingreville. Irradiation resistance of nanostructured interfaces in Zr–Nb metallic multilayers. J. Mater. Res., 34:2239, Jul 2019.

[9] E. Clouet, C. Varvenne, and T. Jourdan. Elastic modeling of point-defects and their interactions. Comp. Mater. Sci., 147:49, 2018.

[10] Jean-Paul Crocombette, Alain Chartier, and William J. Weber. Atomistic simulation of amorphization thermokinetics in lanthanum pyrozirconate. Appl. Phys. Lett., 88(5):051912, 2006.

[11] D. Da Fonseca, F. Onimus, F. Mompiou, M.-C. Marinica, E. de Sonis, E. Clouet, and T. Jourdan. Numerical investigation of dislocation climb under stress and irradiation. Acta Mater., 242:118431, 2023.

[12] C. Domain and C. S. Becquart. Object Kinetic Monte Carlo (OKMC): A Coarse-Grained Approach to Radiation Damage, pages 1–26. Springer International Publishing, 2019.

[13] H Föll and M Wilkens. A simple method for the analysis of dislocation loops by means of the inside-outside contrast on transmission electron micrographs. physica status solidi (a), 31(2):519–524, 1975.

[14] F. A. Garner and D. S. Gelles. Irradiation creep mechanisms: an experimental perspective. J. Nucl. Mater., 159:286, 1988.

[15] F. A. Garner, W. G. Wolfer, and H. R. Brager. A reassessment of the role of stress in development of radiation-induced microstructure. In J. A. Sprague and D. Kramer, editors, Effects of radiation on structural materials, ASTM STP 683, page 160, 1979.

[16] Josselin Garnier, Y Bréchet, M Delnondedieu, C Pokor, P Dubuisson, A Renault, X Averty, and JP Massoud. Irradiation creep of SA 304L and CW 316 stainless steels: Mechanical behaviour and microstructural aspects. Part I: Experimental results. J. Nucl. Mater., 413(2):63–69, 2011.

[17] D. S. Gelles, F. A. Garner, and H. R. Brager. Frank loop formation in irradiated metals in response to applied and internal stresses. In H. R. Brager and J. S. Perrin, editors, Effects of Radiation on Materials: Tenth Conference, ASTM STP 725, page 735, 1981.

[18] N Gharbi, F Onimus, D Gilbon, J-P Mardon, and X Feaugas. Impact of an applied stress on c-component loops under Zr ion irradiation in recrystallized Zircaloy-4 and M5®. J. Nucl. Mater., 467:785–801, 2015.

[19] P. T. Heald and M. V. Speight. Steady-state irradiation creep. Philos. Mag., 29:1075, 1974.

[20] R. V. Hesketh. A transient irradiation creep in non-fissile metals. Philos. Mag., 8:1321, 1963.

[21] S. Jitsukawa, Y. Katano, K. Shiraishi, and F. A. Garner. The Behavior of Irradiation-Produced Dislocation Loops under External Stress during Electron Irradiation. In R. E. Stoller, A. S. Kumar, and D. S. Gelles, editors, Effects of Radiation on Materials: 15th International Symposium, page 1034, 1992.

[22] T Jourdan. Object kinetic monte carlo modelling of irradiation microstructures with elastic interactions. Modell. Simul. Mater. Sci. Eng., 30(8):085013, nov 2022.

[23] G. W. Lewthwaite, D. Mosedale, and I. R. Ward. Irradiation creep in several metals and alloys at 100°C. Nature, 216(5114):472, 1967.

[24] Y. Limoge, A. Rahman, Horngming Hsieh, and Sidney Yip. Computer simulation studies of radiation induced amorphization. J. Non-Cryst. Solids, 99(1):75–88, 1988.

[25] Xiang-Yang Liu, Furio Ercolessi, and James B Adams. Aluminium interatomic potential from density functional theory calculations with improved stacking fault energy. Modell. Simul. Mater. Sci. Eng., 12(4):665, may 2004.

[26] DM Maher and BL Eyre. Neutron irradiation damage in molybdenum. Philosophical Magazine, 23(182):409–438, 1971.

[27] E. Martinez, M. J. Caturla, and J. Marian. DFT-Parameterized Object Kinetic Monte Carlo Simulations of Radiation Damage, page 2457. Springer International Publishing, 2020.

[28] J. R. Matthews and M. W. Finnis. Irradiation creep models – An overview. J. Nucl. Mater., 159:257, 1988.

[29] Frédéric Mompiou and Rui-Xun Xie. pycotem: An open source toolbox for online crystal defect characterization from TEM imaging and diffraction. J. Microsc., 282(1):84–97, 2021.

[30] D. Mosedale, D. R. Harries, J. A. Hudson, G. W. Lewthwaite, and R. J. McElroy. Irradiation creep in fast reactor core component materials. In M. L. Bleiberg and J. W. Bennett, editors, Radiation effects in Breeder Reactor Structural Materials, page 209, 1977.

[31] O. S. Oen. Cross sections for atomic displacements in solids by fast electrons. Technical Report ORNL-4897, ORNL, 1973.

[32] P. R. Okamoto and S. D. Harkness. Stress-biased loop nucleation in irradiated type 316 stainless steels. J. Nucl. Mater., 48:204, 1973.

[33] F. Onimus, T. Jourdan, C. Xu, A. A. Campbell, and M. Griffiths. 1.10 - irradiation creep in materials. In Comprehensive Nuclear Materials, page 310. Elsevier, 2020.

[34] Alexandra Renault-Laborne, J Garnier, J Malaplate, P Gavoille, F Sefta, and B Tanguy. Evolution of microstructure after irradiation creep in several austenitic steels irradiated up to 120 dpa at 320°C. J. Nucl. Mater., 475:209–226, 2016.

[35] Michael J. Sabochick and Nghi Q. Lam. Radiation-induced amorphization of ordered intermetallic compounds CuTi, $CuTi_2$, and Cu_4Ti_3: A molecular-dynamics study. Phys. Rev. B, 43:5243–5252, Mar 1991.

[36] H. Saka, K. Kawamura, Y. Morozumi, and H. Teshima. Effect of external tensile stress on the growth of interstitial loops. J. Nucl. Mater., 179-181:966, 1991.

[37] A. Sato, C. Ikeda, S. Nakamura, M. Suzuki, and T. Mori. Stress effect on formation of interstitial loops in an electron irradiated Fe-18Cr-14Ni alloy. Scr. Metall., 20:1119, 1986.

[38] Alexander Stukowski. Visualization and analysis of atomistic simulation data with OVITO–the Open Visualization Tool. Model. Simul. Mat. Sci. Eng., 18(1):015012, dec 2009.

[39] Alexander Stukowski, Vasily V Bulatov, and Athanasios Arsenlis. Automated identification and indexing of dislocations in crystal interfaces. Model. Simul. Mat. Sci. Eng., 20(8):085007, oct 2012.

[40] M. Suzuki and A. Sato. Stress-assisted nucleation of interstitial loops in an electron-irradiated Fe-18Cr-14Ni alloy. J. Nucl. Mater., 172:97, 1990.

[41] T. Tabata, Y. Nakajima, T. Kida, and H. Fujita. Behavior of lattice defects under the constant load. In Proceedings of the Fifth International Conference on High Voltage, page 519, 1977.

[42] H. Tanigawa, Y. Katoh, and A. Kohyama. Numerical analysis of stress effects on frank loop evolution during irradiation in austenitic Fe-Cr-Ni alloy. Nucl. Instrum. Meth. B, 102:151, 1995.

[43] W. G. Wolfer. Correlation of radiation creep theory with experimental evidence. J. Nucl. Mater., 90:175, 1980.

[44] W. G. Wolfer, L. K. Mansur, and J. A. Sprague. Theory of swelling and irradiation creep. In M. L. Bleiberg and J. W. Bennett, editors, Radiation Effects in Breeder Reactor Structural Materials, page 479, 1977.

[45] C. H. Woo. Irradiation creep due to elastodiffusion. J. Nucl. Mater., 120:55, 1984.

[46] W. Wu and R. Schäublin. The elasticity of the 1/2 a_0 ⟨111⟩ and a_0 ⟨100 dislocation loop in α-Fe thin foil. J. Nucl. Mater, 510:61–69, 2018.

[47] C. Xu and G. S. Was. Anisotropic dislocation loop distribution in alloy T91 during irradiation creep. J. Nucl. Mater., 454:255, 2014.

[48] W.J Yang, R.A Dodd, and G.L Kulcinski. Electron irradiation damage in high purity aluminum. J. Nucl. Mater., 64(1):157–166, 1977.

Supplementary Material for: Evidence of dislocation loop preferential nucleation in irradiated aluminum under stress

D. Da Fonseca[1,5], F. Mompiou[4,5], T. Jourdan[1], J.-P. Crocombette[1], A. Chartier[3], and F. Onimus[2,*]

[1]Université Paris-Saclay, CEA, Service de recherche en Corrosion et Comportement des Matériaux, SRMP, F-91191 Gif-sur-Yvette, France
[2]Université Paris-Saclay, CEA, Service de Recherche en Matériaux et procédés Avancés, F-91191 Gif-sur-Yvette, France
[3]Université Paris-Saclay, CEA, Service de recherche en Corrosion et Comportement des Matériaux, F-91191 Gif-sur-Yvette, France
[4]Centre d'Elaboration de Matériaux et d'Etudes Structurales, CNRS UPR 8011, 29 rue J. Marvig, BP 94347, Toulouse cedex 4 31055, France
[5]Université de Toulouse, UPS, F-31055 Toulouse, France
[*]Corresponding author : fabien.onimus@cea.fr

1 Measurement of sample thickness

The sample thickness was estimated from the length and direction determination of two dislocations emerging at the sample surfaces and located at the periphery of the irradiated area. The procedure is described in [7] using the pycotem software. Measurements of dislocation apparent lengths and directions were obtained at different sample inclination with respect to the main holder axis (here vertical). The apparent thickness at the observation tilt was deduced from dislocation direction and length knowing the electron beam direction. Although the foil normal has not been determined, it was assumed to be close to the beam direction at null tilt. The thickness ranges from 210±16 nm to 137±16 nm for the two dislocations, indicating that the foil has a wedge shape. For the sake of simplicity, we took an average thickness of 170 nm.

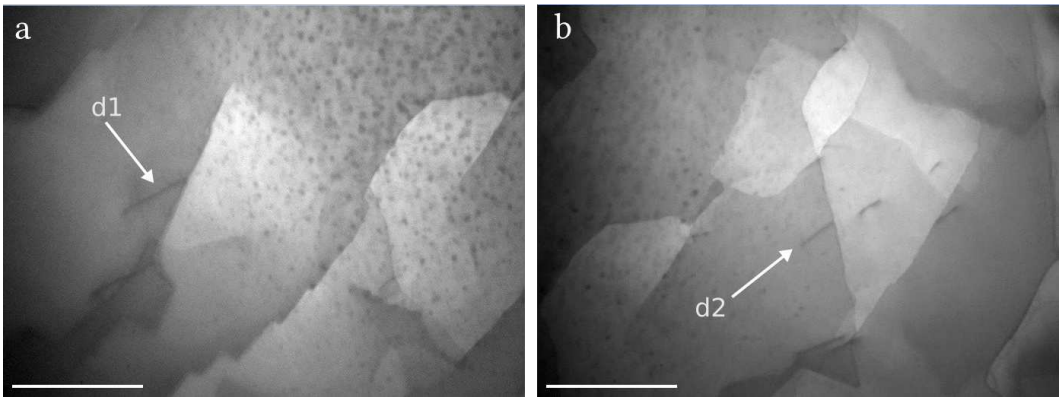

Figure 1: Two micrographs showing two dislocations of interest *d1* and *d2* for thickness determination: (a) left part of the irradiation area, where the sample is thicker because it is further away from the electropolished hole and (b) right part of the irradiation area, closer to the hole. Scale bars correspond to 500 nm.

2 Measurement of local stress

The local stress applied during the in-situ TEM experiments was evaluated in-situ between experiment 3.a and 3.b (see letter) using the dislocation curvature of the first moving dislocation. In this area, the principal local stress is a tensile stress with an axis parallel to the sample holder as indicated in Fig. 2. First, the sample was strained, by increasing the displacement of the mobile grip, until dislocation glide was observed in the same grain where irradiation experiments were performed. Then the grip displacement was slightly reduced to stop the dislocation motion before the stress was relaxed Fig. 2.a. The glide plane, $(1\,1\,1)$, was deduced from slip traces analysis knowing crystal orientation and thickness using pycotem [7]. Cross-slip was eventually observed in the $(0\,0\,1)$ plane deduced from its trace analysis Fig. 2.c. The Burgers vector is then at the intersection of the two planes, i.e. along the $\langle 1\,\bar{1}\,0\rangle$ direction as shown in the stereographic projection in Fig. 2.b. The local shear stress was inferred from the comparison between the shape of a dislocation at a given stress computed from anisotropic elasticity, using DISDI [4] and elastic constants at 300 K from [8], and its shape on an image corrected from perspective effect (Fig. 2.d). We estimate the local shear stress to be equal to 45 ± 5 MPa (Fig. 2.d). Considering a Schmid factor of 0.47 and that the stress is locally a pure tensile stress, the applied stress is estimated to be between 85 and 106 MPa.

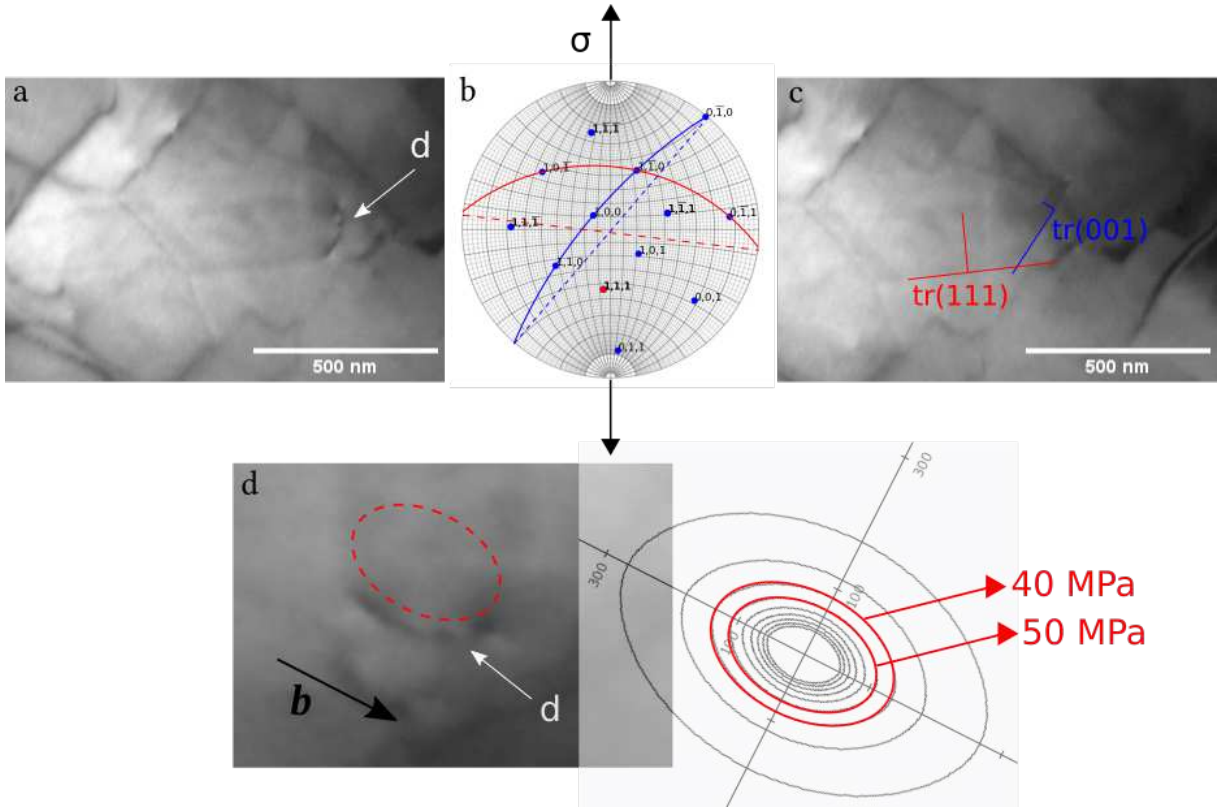

Figure 2: (a) Micrograph showing a curved gliding dislocation *d*. The slip traces left at sample surfaces are visible on the dislocation wake after its motion from left to right. (b) Stereographic projection of the crystal as observed. (c) Micrograph showing the cross-slip of dislocation *d*. Primary and cross-slip traces are highlighted in red and blue respectively. Their apparent widths are also indicated perpendicular to the traces. They match the plane shown in the stereographic projection. (d) Image of the dislocation corrected from perspective effect and the best theoretical shape. The fit was chosen from a series of theoretical shapes when varying the applied shear stress from 20 to 100 MPa with 10 MPa step (right). The local tensile axis is reported on the stereographic projection.

3 OKMC parametrization

In our simulations only point defects are assumed to migrate. Migration energies in the bulk, without any effect of stress, are 0.105 eV for self-interstitial atoms and 0.605 eV for vacancies [1]. Elastic properties of point defects (elastic dipoles and polarizabilities), which affect their mobility under stress, are given in Ref. [3]. Including the mobility of small point defects clusters would not change the results. The concentration of SIAs is so low that no di-interstitials form. Vacancies are assumed not to bind together, in agreement with DFT calculations [9, 2]. Only SIA-impurity and vacancy-impurity complexes may form, which are assumed to be immobile. SIA-impurity binding energy is chosen equal to 1 eV in order to avoid any thermal dissociation. The binding energy of vacancy-impurity is assumed to be lower than the latter. It is chosen to equal to 0.4 eV. It is probably an upper bound for the binding energy with impurities [5]. With such a value, some cavities may form occasionally but their number is far lower than loops. This proves that cavities should not be seen, as confirmed experimentally.

SIA-impurity and vacancy-impurity clusters can grow by absorbing SIAs and vacancies, respectively. Clusters containing 2 SIAs or more are modelled as Frank loops. No thermal emission of point defects from these loops is permitted. This approximation is well justified given the low temperature at which simulations are performed. The binding energy of a vacancy with a vacancy cluster, nucleated on an impurity and modelled as a cavity, is equal to the binding energy with the impurity (0.4 eV) if the number of vacancies attached to the impurity is smaller than the number of first nearest neighbours of the impurity (assumed to be equal to 12) or if the binding energy with the impurity is higher than the binding energy with a cavity. This binding energy, which is used otherwise, is calculated with a capillary law [6] based on the binding energy of 2 vacancies (0 eV) and the formation energy of a vacancy (0.67 eV).

Vacancies and SIAs are created as Frenkel pairs, at a distance of $4a$, where a is the lattice parameter. They are described as spherical defects of radius 0.16 nm, which recombine with each other if the distance between their center is lower than $2a$. They agglomerate with a Frank dislocation loop if the distance to the dislocation line is lower than $2b$, where b is the Burgers vector of the loop.

References

[1] D. Carpentier, T. Jourdan, Y. Le Bouar, and M.-C. Marinica. Effect of saddle point anisotropy of point defects on their absorption by dislocations and cavities. Acta Mater., 136:323, 2017.

[2] D. Connétable and M. David. Study of vacancy-(H,B,C,N,O) clusters in Al using DFT and statistical approaches: Consequences on solubility of solutes. J. Alloys Compd., 748:12, 2018.

[3] D. Da Fonseca, F. Onimus, F. Mompiou, M.-C. Marinica, E. de Sonis, E. Clouet, and T. Jourdan. Numerical investigation of dislocation climb under stress and irradiation. Acta Mater., 242:118431, 2023.

[4] J. Douin, P. Veyssière, and P. Beauchamp. Dislocation line stability in Ni_3Al. Philos. Mag., 54(3):375–393, 1986.

[5] P. Ehrhart, P. Jung, H. Schultz, and H. Ullmaier. Landolt–Börnstein, Numerical Data and Functional Relationships in Science and Technology. Atomic Defects In Metals. Springer, 1991.

[6] C. C. Fu, F. Willaime, and P. Ordejón. Stability and mobility of mono- and di-interstitials in α-Fe. Phys. Rev. Lett., 92:175503, 2004.

[7] Frédéric Mompiou and Rui-Xun Xie. pycotem: An open source toolbox for online crystal defect characterization from TEM imaging and diffraction. J. Microsc., 282(1):84–97, 2021.

[8] J. Vallin, M. Mongy, K. Salama, and O. Beckman. Elastic constants of aluminum. J. Appl. Phys., 35(6):1825–1826, 1964.

[9] H. Wang, D. Rodney, D. Xu, R. Yang, and P. Veyssière. Pentavacancy as the key nucleus for vacancy clustering in aluminum. Phys. Rev. B, 84:220103, 2011.